Journal of Molecular Catalysis A: Chemical 320 (2010) 97–105

Contents lists available at ScienceDirect

Journal of Molecular Catalysis A: Chemical

journal homepage: www.elsevier.com/locate/molcata

Understanding the deposition–precipitation process for the preparation of supported Au catalysts

Kun Qian[a,b], Jun Fang[a,b], Weixin Huang[a,b,*], Bo He[c], Zhiquan Jiang[a,b], Yunsheng Ma[a,b], Shiqiang Wei[c]

[a] Hefei National Laboratory for Physical Sciences at the Microscale, Hefei 230026, China
[b] CAS Key Laboratory of Materials for Energy Conversion and Department of Chemical Physics, University of Science and Technology of China, Hefei 230026, China
[c] National Synchrotron Radiation Laboratory, University of Science and Technology of China, Hefei 230029, China

ARTICLE INFO

Article history:
Received 25 September 2009
Received in revised form 20 January 2010
Accepted 21 January 2010
Available online 28 January 2010

Keywords:
$Au/CoO/SiO_2$ catalysts
CO oxidation
Deposition–precipitation
Metal–support interaction
Surface hydroxyls

ABSTRACT

We have employed the deposition–precipitation method to prepare $Au/CoO/SiO_2$ catalysts. The structure and activity of $Au/CoO/SiO_2$ catalysts in CO oxidation were found to depend on the Au:CoO ratio. The catalyst preparation process was investigated employing in situ infrared spectroscopy. The gold precursor preferentially deposits and interacts with hydrogen-bonded hydroxyls and then with isolated hydroxyls in $Co(OH)_2$ on SiO_2, eventually forming large and fine Au nanoparticles in the catalysts, respectively. The calcination of SiO_2 at 500 °C prior to the catalyst preparation can alter the structure of Au nanoparticles in $Au/CoO/SiO_2$ catalysts by changing the distribution of hydrogen-bonded and isolated hydroxyls in $Co(OH)_2$. $Au/CoO/SiO_2$ catalysts with fine Au nanoparticles are active in low temperature CO oxidation. Our results provide direct evidence that the interaction between the gold precursor and surface hydroxyls on the support during the deposition–precipitation process plays an important role in determining the structure of supported Au nanoparticles.

1. Introduction

In 1989, Haruta et al. firstly reported that the ultrafine Au particles supported on transition metal oxides exhibited exceptionally high activity in CO oxidation at low temperature [1], which sparked off intensive research in gold catalysis. Gold has been demonstrated as a unique heterogeneous or homogeneous catalyst in a wide array of reactions [2–4]. Supported Au nanoparticles-catalyzed low temperature CO oxidation is the most intensively investigated system not only because of its potential for practical applications but also because of an expectation that a thorough understanding of this apparently simple reaction could serve as a platform to understand other gold-catalyzed complex reactions. Although extensive experimental and theoretical studies have been made in the fundamental understanding of this system, there still remain some ambiguous issues, particularly with respect to the nature of the active site, the role of the oxide support, and the reaction mechanism [5–11]. The situation can be partly explained by different experimental conditions employed in various studies, which leads to the diversity in the proposed explanations. For example, the surface science studies of model catalysts under ultra-high vacuum conditions often observe that oxygen vacancies in the oxide supports can transfer charge to supported Au clusters, forming negatively charged Au clusters that have been proposed as part of the active sites [12–16]. However, the practical supported powder catalysts are usually prepared by wet-chemical methods employing fully oxidized supports, in which cationic gold species has been often observed and proposed as part of the active sites [17–20]. A well-established structure-activity relation in supported Au catalysts for low temperature CO oxidation is the size-dependent activity, in which fine Au nanoparticles are usually more active than large Au nanoparticles.

It is generally accepted that the structure and the activity of supported Au nanoparticles are highly sensitive to the employed preparation procedure [6]; this sometimes makes it difficult for the reproducible preparation of supported Au catalyst by different research groups [10]. Deposition–precipitation (DP) and coprecipitation are two routine methods to prepare active supported Au catalysts employing aqueous $HAuCl_4$ as the gold precursor [21]. There are a lot of reports [22–36] investigating the influence of the preparation variables, such as the pH value of aqueous $HAuCl_4$ solution, the precipitation agent and the calcination temperature, on the structures and catalytic activities of Au nanoparticles. However, most of these studies emphasize on the characterization and catalytic performance of supported Au catalysts. Only several studies [24,28,29] pay attention to the preparation process itself, which all investigated the influence of pH-dependent species of Au complexes on the structure and activity of supported Au catalysts.

* Corresponding author at: Department of Chemical Physics, University of Science and Technology of China, Jinzhai Road 96, Hefei 230026, China.
Tel.: +86 551 3600435; fax: +86 551 3600437.
E-mail address: huangwx@ustc.edu.cn (W. Huang).

1381-1169/$ – see front matter © 2010 Elsevier B.V. All rights reserved.
doi:10.1016/j.molcata.2010.01.010

Yang et al. [28] employed extended X-ray absorption fine structure (EXAFS) and transmission electron microscope (TEM) to characterize key steps in the preparation of Au/Al_2O_3 catalysts in conjunction with activity measurements and found that the residual chloride affected largely the catalytic activity. Moreau et al. [29] found that the optimum pH for the preparation of highly active Au/TiO_2 catalysts is about 9, under which most of chlorine in the anionic complexes were removed by hydrolysis. Zanello et al. [24] reported that different gold species were formed in the aqueous solution and deposited on the TiO_2 surface when preparing Au/TiO_2 catalysts with urea and NaOH as the precipitation agent. However, due to the complexity of the catalyst preparation process, they still remain unclear how the gold precursor interacts with the support surface and how the precursor–support interaction affects the structure of supported Au nanoparticles.

The transition metal oxide supported Au catalysts in which only the Au loading could be varied are not very suitable for the investigation of the gold precursor–support interaction. It is desirable that both the loadings of Au and transition metal oxide could be varied in the catalysts so that the gold precursor–support interaction and its influence on the structure of supported Au nanoparticles could be manifested. We recently developed a convenient DP method to load Au nanoparticles and transition metal oxides on SiO_2 surface ($Au/MO_x/SiO_2$), which were active in low temperature CO oxidation [37,38]. SiO_2 is an inert support [39] and Au/SiO_2 catalysts prepared by the routine methods are not active in low temperature CO oxidation [40–42]. In our $Au/MO_x/SiO_2$ catalysts, the activity in low temperature CO oxidation arises from Au nanoparticles supported on transition metal oxides, moreover, the loadings of gold and transition metal oxide are comparable. Therefore, the $Au/MO_x/SiO_2$ catalyst provides an ideal catalyst system for the investigation of the gold precursor–transition metal oxide interaction and its influence on the structure and catalytic activity of Au nanoparticles. In this paper, we report a detailed investigation of $Au/CoO/SiO_2$ catalysts with different Au and CoO loadings. It is found that the structure of supported Au nanoparticles and the activity of $Au/CoO/SiO_2$ catalysts in CO oxidation depend sensitively on the Au:CoO ratio and we proposed that the interaction between the gold precursor and surface hydroxyls on the support during the DP process plays an important role in determining the structure of supported Au nanoparticles.

2. Experimental

Typically, SiO_2 (40–120 mesh, Qingdao Haiyang Chemicals Co.) was first modified with $Co(NO_3)_2$ by the conventional incipient wetness impregnation method (using $Co(NO_3)_2{\cdot}6H_2O$ (Sinopharm Chemical Reagent Co., Ltd, ≥99.0%) as the cobalt precursor) followed by drying at 60 °C overnight. The resulting support was then directly used for the preparation of $Au/CoO/SiO_2$ catalysts by the routine DP method using $HAuCl_4{\cdot}4H_2O$ (Sinopharm Chemical Reagent Co., Ltd, Au content ≥ 47.8%) as the gold precursor. The calculated amount of $HAuCl_4{\cdot}4H_2O$ aqueous solution was added into a three-neck bottle containing the support, and then ammonia water was slowly added to adjust the pH between 9 and 10. The system was stirred at 60 °C for 24 h. Then the precipitate was filtered and washed several times. The resulting powder was dried at 60 °C overnight, followed by calcination at 200 °C under the ambient condition for 4 h. For comparison, we also prepared Au/SiO_2 and CoO/SiO_2 catalysts in a similar method. To investigate the effect of surface hydroxyl of SiO_2 support, SiO_2 calcined at 500 °C under the ambient condition for 4 h prior to the catalyst preparation was also employed as the support, as described in the following section.

The loadings of Au and Co in the catalysts were analyzed by an inductively coupled plasma atomic emission spectrometer (ICP-AES). BET surface areas of the catalysts were measured on a Beckman Coulter SA3100 Surface Area Analyzer, in which the sample was degassed at 120 °C for 30 min in the nitrogen atmosphere prior to the measurement. Powder X-ray diffraction (XRD) patterns were acquired on a Philips X'Pert PRO SUPER X-ray diffractometer with a Ni-filtered Cu Kα X-ray source operating at 40 kV and 50 mA. TEM experiments were preformed on a JEOL 2010 high-resolution transmission electron microscope with the energy dispersive spectrum (EDS) analysis facility. High-resolution X-ray photoelectron spectroscopy (XPS) measurements were performed on an ESCALAB 250 high performance electron spectrometer using monochromatized Al Kα excitation source ($h\nu = 1486.6$ eV)). The binding energies in the XPS spectra were referenced to the Si 2p binding energy in SiO_2 at 103.3 eV. The infrared (IR) spectra were recorded on a MAGNA-IR 750 Fourier transformed infrared spectrometer with a home-made heating apparatus that allowed for the in situ measurement of IR spectrum during the course of sample heating.

X-ray absorption spectroscopy (XAS) measurements for the Au L_{III}-edge (11,719–12,919 eV) and the Co K-edge (7609–8709 eV) were performed in the transmission mode at room temperature on the XAS Station of the U7C beam line of National Synchrotron Radiation Laboratory (NSRL, Hefei, China). The synchrotron radiation facility mainly consists of an 800 MeV electron storage ring with the ring current of about 100–300 mA. A Si(1 1 1) double-crystal was used as the monochromator. The X-ray absorption near edge structure (XANES) spectra were acquired at a 0.7-eV energy step.

The catalytic activities of $Au/CoO/SiO_2$ catalysts in CO oxidation were evaluated in a fixed-bed flow reactor without any pre-treatment. The catalyst weight was 100 mg and the reaction gas consisting of 1% CO and 99% dry air was fed at a rate of 20 ml/min. The steady-state composition of the effluent gas was analyzed with an online GC-14C gas chromatograph equipped with a TDX-01 column ($T = 80$ °C, H_2 as the carrier gas at 30 ml/min) after the catalytic reaction operated at desirable reaction temperatures for 30 min. The conversion of CO was calculated from the difference of CO concentrations in the inlet and outlet gases.

3. Results and discussion

Two series of $Au/CoO/SiO_2$ catalysts were prepared whose compositions and BET surface areas are summarized in Table 1. One series is with a nearly-fixed CoO loading (Co:SiO_2 weight ratio: 6%) and variable Au loadings, in which six catalysts with increasing Au loading are denoted as Au/6%-CoO/SiO_2-*x* (*x* represents the number of 1–6). The other series is with a similar Au loading (Au:SiO_2 weight ratio: 1%) and variable CoO loadings, in which five catalysts with increasing Co loading are denoted as 1%-Au/CoO/SiO_2-*x* (*x* represents the number of 1–5). Based on Table 1, it is shown that various Au/6%-CoO/SiO_2 catalysts are with similar BET surface areas, so are various 1%-Au/CoO/SiO_2 catalysts.

Fig. 1A shows catalytic activities of various Au/6%-CoO/SiO_2 catalysts in CO oxidation. Both Au/SiO_2 and 6%-CoO/SiO_2 catalysts perform poorly in CO oxidation. The catalytic activity of Au/6%-CoO/SiO_2 catalysts is much better than that of Au/SiO_2 and 6%-CoO/SiO_2, but depends on the Au loading, i.e. the Au:CoO ratio. In general, the catalysts with higher Au loading are more active. The catalytic activities for CO oxidation at room temperature are observed for Au/6%-CoO/SiO_2-3 and those with higher Au loadings, but not for Au/6%-CoO/SiO_2-1 and Au/6%-CoO/SiO_2-2. The specific rate of CO conversion catalyzed by Au/6%-CoO/SiO_2-3 and Au/6%-CoO/SiO_2-4 at room temperature, for example, was calculated to be 0.154 and 0.165 $mol_{CO}\ g_{Au}^{-1}\ h^{-1}$, respectively.

The activities of various 1%-Au/CoO/SiO_2 catalysts show a similar dependence on the Au:CoO ratio (Fig. 1B). Both 1%-Au/CoO/SiO_2-1 and 1%-Au/CoO/SiO_2-2 are active in low temperature CO oxidation, and 1%-Au/CoO/SiO_2-2 with a lower

Table 1
Structural parameters of various catalysts.

Catalyst	BET surface area (m^2/g)	Weight ratio		Average size of Au nanoparticles (nm)	
		Au/SiO_2 (%)	Co/SiO_2 (%)	d_{XRD}	d_{TEM}[a]
Au/SiO_2	316	1.0	N.A.	12	9.0
Au/6%-CoO/SiO_2-1	327	0.6	6.0	11	N.M.
Au/6%-CoO/SiO_2-2	315	1.6	5.8	18	[b]
Au/6%-CoO/SiO_2-3	261	2.6	6.6	24	4.3
Au/6%-CoO/SiO_2-4	278	3.0	5.9	31	N.M.
Au/6%-CoO/SiO_2-5	243	5.4	5.6	41	5.6
Au/6%-CoO/SiO_2-6	306	7.5	6.0	10	6.5
1%-Au/CoO/SiO_2-1	296	0.7	0.9	7	N.M.
1%-Au/CoO/SiO_2-2	301	0.9	1.8	33	4.6[c]
1%-Au/CoO/SiO_2-3	273	0.9	3.8	36	N.M.
1%-Au/CoO/SiO_2-4	283	0.9	5.4	35	N.M.
1%-Au/CoO/SiO_2-5	319	0.8	7.4	23	N.M.

N.A.: not applicable; N.M.: not measured.
[a] Only Au nanoparticles finer than 15 nm observed in TEM images were considered.
[b] No Au nanoparticles finer than 15 nm.
[c] Amount of Au nanoparticles less than 100.

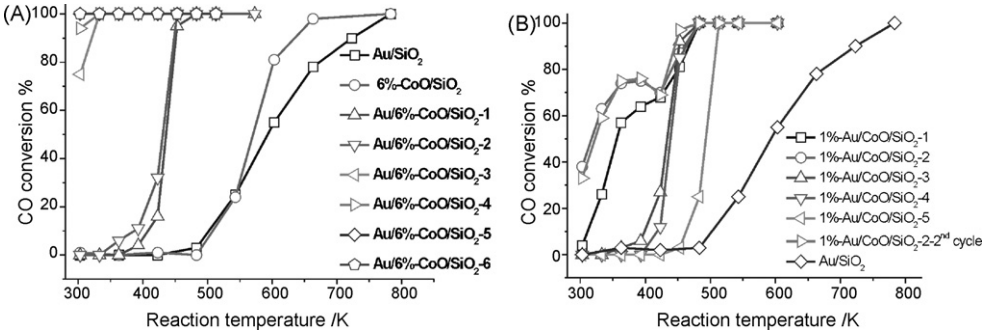

Fig. 1. Catalytic performances of (A) Au/6%-CoO/SiO_2 and (B) 1%-Au/CoO/SiO_2 catalysts in CO oxidation.

Au:CoO ratio is more active than 1%-Au/CoO/SiO_2-1 with a higher Au:CoO ratio. However, with further decreasing Au:CoO ratio, 1%-Au/CoO/SiO_2 catalysts become inactive in low temperature CO oxidation. The specific rate of CO conversion catalyzed by 1%-Au/CoO/SiO_2-1 and 1%-Au/CoO/SiO_2-2 at room temperature was calculated to be 0.028 and 0.208 $mol_{CO}\, g_{Au}^{-1}\, h^{-1}$, respectively. An interesting observation is that the catalytic activity of 1%-Au/CoO/SiO_2-1 and 1%-Au/CoO/SiO_2-2 shows a volcano-shape dependence on the reaction temperature within the range from RT to 150 °C, which was not observed in Au/6%-CoO/SiO_2 catalysts. Such a behavior was reproducible for the tested 1%-Au/CoO/SiO_2-2 catalyst when we repeated the above temperature-dependent activity measurements. This indicates that the observed activity-reaction temperature dependence cannot be attributed to the structural variation of the catalyst during the course of activity measurement.

Above results demonstrate that the activities of Au/CoO/SiO_2 catalysts in CO oxidation are largely dependent on the Au:CoO ratio. The Au/CoO/SiO_2 catalysts with low Au:CoO ratios are relatively more active than Au/SiO_2 and CoO/SiO_2 in CO oxidation but do not show any activities at low temperatures (<400 K). In contrast, Au/CoO/SiO_2 catalysts with high Au:CoO ratios are active for CO oxidation even at room temperature. Fig. 2 displays the XRD patterns of various Au/CoO/SiO_2 catalysts. All the observed diffraction peaks could be well indexed to Au. No diffraction peaks arising from CoO were observed, indicating the high dispersion of CoO on SiO_2. The Au diffraction peaks grow and narrow as the Au loading of Au/6%-CoO/SiO_2 catalysts increases, but unexpectedly

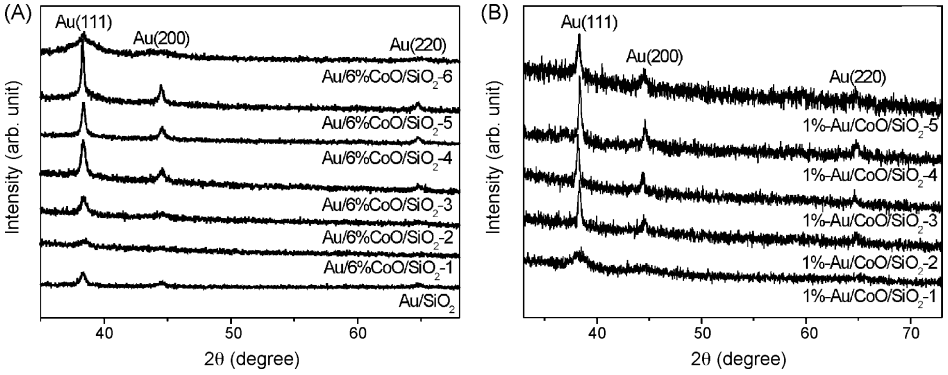

Fig. 2. XRD patterns of (A) Au/6%-CoO/SiO_2 catalysts and (B) 1%-Au/CoO/SiO_2 catalysts.

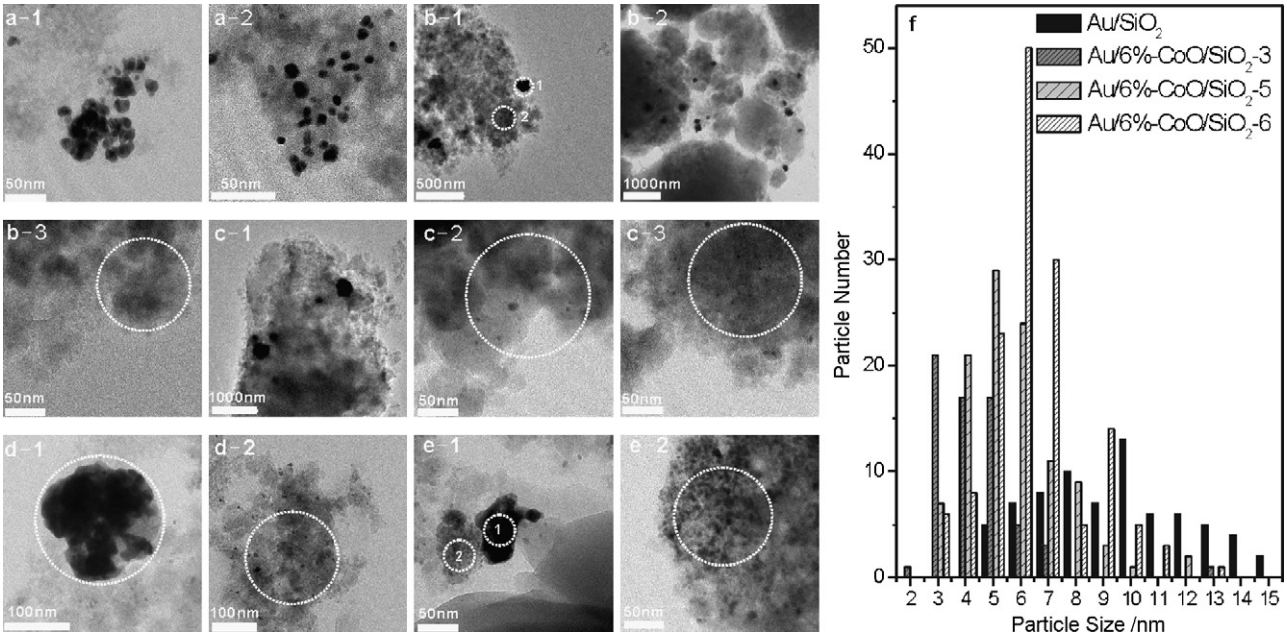

Fig. 3. TEM images of (a) Au/SiO_2; (b) $Au/6\%\text{-}CoO/SiO_2$-2; (c) $Au/6\%\text{-}CoO/SiO_2$-3; (d) $Au/6\%\text{-}CoO/SiO_2$-5; (e) $Au/6\%\text{-}CoO/SiO_2$-6, and (f) the size distribution of supported Au nanoparticles finer than 15 nm in indicated catalysts. The dash circles indicated in the TEM images show the areas whose compositions were examined by EDS (Fig. S1).

broaden for $Au/6\%\text{-}CoO/SiO_2$-6. For the $1\%\text{-}Au/CoO/SiO_2$ catalysts, $1\%\text{-}Au/CoO/SiO_2$-1 displays rather broad diffraction peaks, but $1\%\text{-}Au/CoO/SiO_2$ catalysts with higher CoO loadings all exhibit sharp diffraction peaks. The average crystalline sizes of Au nanoparticles in the catalysts were calculated from the full width at half maximum (FWHM) of Au(1 1 1) diffraction peak and the results were summarized in Table 1. Obviously, the average crystalline sizes of supported Au nanoparticles are not consistent with the general observation that only fine Au nanoparticles (~5 nm) exhibit activity in low temperature CO oxidation. Thus TEM was used to detect the true size distributions of Au nanoparticles in our catalysts, whose results are shown in Figs. 3 and 4.

Au nanoparticles in Au/SiO_2 are mostly with sizes around 10 nm. Only large Au aggregates were observed in $Au/6\%\text{-}CoO/SiO_2$-2 with a 1.6% Au loading and no well-dispersed fine Au nanoparticles could be found. The EDS analysis results (Fig. S1) of areas indicated in Fig. 3b-1 and b-3 further prove the absence of fine Au nanoparticles in $Au/6\%\text{-}CoO/SiO_2$-2. In the TEM images of $Au/6\%\text{-}CoO/SiO_2$-3 with an Au loading of 2.6%, large Au aggregates are still present but fine Au nanoparticles could be clearly observed. The density of fine Au nanoparticles in $Au/6\%\text{-}CoO/SiO_2$ catalysts increases with further increasing Au loading, but large Au aggregates are always present. We counted the size distribution of Au nanoparticles finer than 15 nm in these catalysts observed by TEM (Fig. 3f), from which the average size of Au nanoparticles was calculated to be 10.4, 4.3, 5.6, and 6.5 nm in Au/SiO_2, $Au/6\%\text{-}CoO/SiO_2$-3, $Au/6\%\text{-}CoO/SiO_2$-5, and $Au/6\%\text{-}CoO/SiO_2$-6, respectively. The elemental composition of areas containing fine Au nanoparticles and large Au aggregates indicated in the TEM images was further analyzed by EDS (Fig. S1). It could be seen that areas containing large Au aggregates have high Au:CoO ratios whereas those containing fine Au nanoparticles have low Au:CoO ratios. Considering that the detection depth of EDS is ca. 300–400 nm, therefore, large Au aggregates should not have much influence on the detection of the underlying CoO. The TEM images of $1\%\text{-}Au/CoO/SiO_2$-2 (Fig. 4) also demonstrate the coexistence of large Au aggregates and fine Au nanoparticles (particles indicated by dotted circles in Fig. 4). These TEM results clearly show that the size of Au nanoparticles in $Au/CoO/SiO_2$ catalyst depends on the Au:CoO ratio. $Au/CoO/SiO_2$ catalysts with low Au:CoO ratios only contain large Au aggregates whereas $Au/CoO/SiO_2$ catalysts

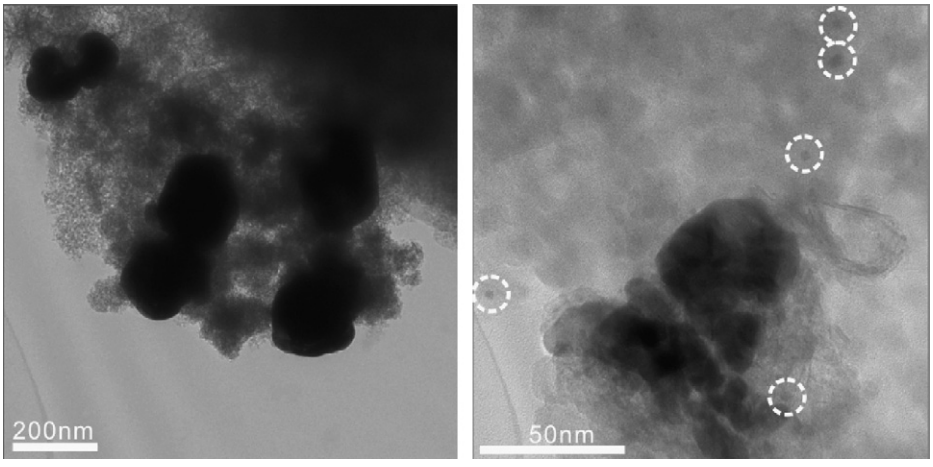

Fig. 4. TEM images of $1\%\text{-}Au/CoO/SiO_2$-2. The fine Au nanoparticles are indicated by dotted circles.

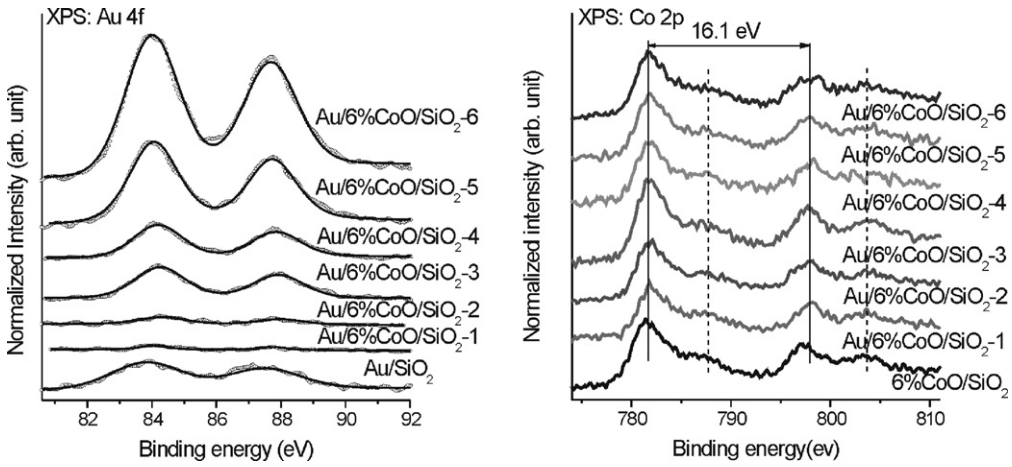

Fig. 5. Au 4f and Co 2p XPS spectra of various Au/6%-CoO/SiO_2 catalysts. The scatter points and solid line in the Au 4f XPS spectra correspond to the original and fitted spectrum, respectively.

with high Au:CoO ratios demonstrate a bi-modal size distribution of Au nanoparticles. The existence of fine Au nanoparticles in Au/CoO/SiO_2 catalysts with high Au:CoO ratios explains well the observed activity of these catalysts in low temperature CO oxidation (Fig. 1).

Fig. 5 shows the Au 4f and Co 2p XPS spectra of various catalysts. The Au 4f XPS peak intensity increases with an increase of Au loading in Au/6%-CoO/SiO_2 catalysts. The Au 4f XPS peak of Au/6%-CoO/SiO_2 catalysts could be well fitted with one component with the Au $4f_{7/2}$ binding energy at ca. 84.0 eV, implying that only metallic Au exists in the catalysts. The Co 2p XPS spectra of these catalysts are similar, showing the Co $2p_{3/2}$ binding energy at 781.7 eV, the $2p_{3/2}$–$2p_{1/2}$ spin–orbit splitting (ΔE) of 16.1 eV, and an obvious satellite peak at the high-energy side. CoO and Co_3O_4 show similar Co 2p binding energy, but the Co $2p_{3/2}$–$2p_{1/2}$ spin–orbit splitting (ΔE) is 15.0 eV for Co_3O_4 and 15.7 eV for CoO [43] and a shoulder at the high-energy side, which has to be traced back to a shake-up process, could only be observed in the high spin Co^{2+} ion but not in the diamagnetic low-spin Co^{3+} ion [44]. Thus the XPS results indicate that the Co species is essentially CoO in the catalysts. The electronic structures of Au and Co in the catalysts were further investigated by XAS. Fig. 6 presents the Au L_{III}-edge and Co K-edge XANES spectra of selected catalysts. The Au L_{III}-edge XANES spectrum is very sensitive in detecting Au cations which exhibits a strong peak at 11,921.6 eV. This feature corresponds to the white line position of Au due to a $2p_{3/2} \rightarrow 5d$ transition, and its intensity is proportional to the density of unoccupied d states and thus decreases with the reducing oxidation state of Au [45]. It could be clearly seen that Au/SiO_2, Au/6%-CoO/SiO_2-2, and Au/6%-CoO/SiO_2-6 show the nearly identical Au L_{III}-edge XANES spectra: the adsorption edge at 11,919 eV, a shoulder at 11,933 eV, and two peaks at 11,949 and 11,973 eV. These features are the characteristics of the XANES spectrum of metallic Au [31], demonstrating that the gold species in these catalysts is metallic. Meanwhile, comparing with those of CoO and Co_3O_4, the Co K-edge XANES spectra of Au/6%-CoO/SiO_2-2 and Au/6%-CoO/SiO_2-6 suggest that the Co species in the catalysts is CoO. These XANES results agree very well with XPS results.

The Au 4f and Co 2p XPS spectra of various 1%-Au/CoO/SiO_2 catalysts are presented in Fig. 7, also demonstrating the existence of metallic Au and CoO. It could be seen that the normalized Au 4f XPS peak area obviously reduces as the Au:CoO ratio decreases from

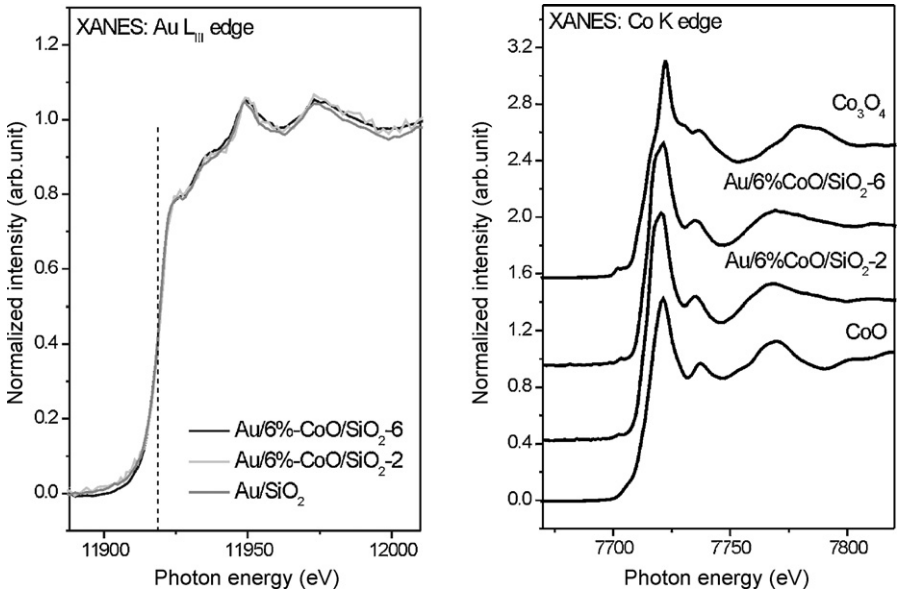

Fig. 6. XANES spectra of Au L_{III}-edge and Co K-edge of indicated catalysts.

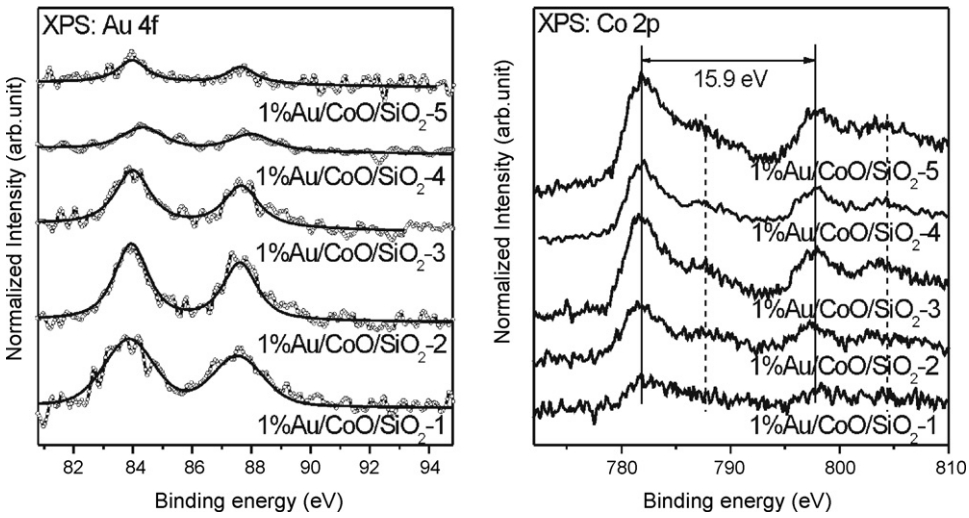

Fig. 7. Au 4f and Co 2p XPS spectra of various 1%-Au/CoO/SiO_2 catalysts. The scatter points and solid line in the Au 4f XPS spectra correspond to the original and fitted spectrum, respectively.

the value of 1%-Au/CoO/SiO_2-1 to that of 1%-Au/CoO/SiO_2-5. Since these catalysts have a similar Au loading, this observation indicates that the dispersion of Au particles become worse with low Au:CoO ratio, consistent with the above TEM results (Fig. 3).

Therefore, by systematically varying the Au:CoO ratio in Au/CoO/SiO_2 catalysts, Au/CoO/SiO_2 catalysts exemplify well the general observation that fine Au nanoparticles are active in low temperature CO oxidation. More importantly, Au/CoO/SiO_2 catalysts demonstrate a very interesting size distribution of Au nanoparticles depending on the Au:CoO ratio. Large Au nanoparticles preferentially form in Au/CoO/SiO_2 catalysts with low Au:CoO ratios, such as Au/6%-CoO/SiO_2-1, Au/6%-CoO/SiO_2-2, 1%-Au/CoO-SiO_2-3, 1%-Au/CoO-SiO_2-4, and 1%-Au/CoO-SiO_2-5; with increasing Au:CoO ratio, fine Au nanoparticles appear and eventually dominate in the catalysts, but large Au nanoparticles are always present. These observations may suggest that there are two kinds of nucleation sites on the support for the gold precursor during the course of catalyst preparation, leading to the formation of large Au nanoparticles and fine Au nanoparticles. Moreover, the gold precursor preferentially nucleates on the site leading to the formation of large Au nanoparticles.

During the DP process at pH between 9 and 10, the gold precursor mainly consists of $[AuCl(OH)_3]^-$ and $[Au(OH)_4]^-$ [31,46,47], and the used $Co(NO_3)_2/SiO_2$ is transformed to $Co(OH)_2/SiO_2$. Therefore, it is the interaction among these species determining the nucleation and growth of Au nanoparticles. The gold precursor was proposed to deposit and interact with hydroxyls on the oxide support surface when preparing supported Au catalysts by the DP method [24,29], in which the point of zero charge (PZC) and surface hydroxyls of oxide support played important roles. The PZC of SiO_2 is ~2 and that of $Co(OH)_2$ is ~11.4, therefore, the surface of SiO_2 is seriously negatively charged under the employed preparation condition; meanwhile, $Co(OH)_2$ could provide more surface hydroxyls than SiO_2. Therefore, it is reasonable that the gold precursor deposits and interacts with $Co(OH)_2$ of $Co(OH)_2/SiO_2$. This also agrees with the EDS experimental results (Fig. S1) that areas containing either large Au aggregates or fine Au nanoparticles in the TEM images always contain CoO no matter what the CoO loading is in Au/CoO/SiO_2 catalysts. Meanwhile, the areas with large Au aggregates always contain high concentrations of Co whereas those with fine Au nanoparticles contain low concentrations of Co.

In order to understand the Au:CoO ratio-dependent size distribution of Au nanoparticles in Au/CoO/SiO_2 catalysts, we studied the preparation process by means of the in situ IR spectroscopy that can measure the IR spectrum of samples during the course of heating in an ambient atmosphere. We first studied the preparation process of CoO/SiO_2 supports (Fig. 8A). The vibrational band at ~960 cm^{-1} arising from the Si–O stretch vibration of Si–OH on SiO_2 [48] attenuates when SiO_2 is calcined at 200 °C. The loading of $Co(OH)_2$ on SiO_2 leads to the obvious weakening of the Si–O stretch vibration peak of Si–OH. This suggests that Co(II) of $Co(NO_3)_2$ exchanges with H^+ of Si–OH during the impregnation step and then transforms to $Co(OH)_2$ during the following DP step.

Fig. 8B shows the O–H stretch vibration spectra of various samples that were recorded at 200 °C. The bare SiO_2 support shows a broad vibrational peak centering at ~3376 cm^{-1} accompanied by a narrow shoulder peak at ~3638 cm^{-1}, which could be assigned to the O–H stretch vibration of hydrogen-bonded and isolated surface hydroxyls on SiO_2, respectively [49]. The narrow peak at ~3638 cm^{-1} obviously gains intensity after the loading of 6%-CoO on the SiO_2 support, which might arise from isolated surface hydroxyls on CoO resulted from the decomposition of supported $Co(OH)_2$. It has been reported that hydrogen-bonded and isolated hydroxyl groups in $Co(OH)_2$ show the O–H stretch vibration band at ~3450 and ~3630 cm^{-1}, respectively [50]. Interestingly, the intensity of the narrow vibrational peak weakens only slightly in Au/6%-CoO/SiO_2-2 but very substantially in Au/6%-CoO/SiO_2-6. In order to give the quantitative information, the IR spectra in Fig. 8B were fitted with the assumption that there are two components arising from isolated surface hydroxyls and other forms of hydroxyls. These two components are with the same peak shape and the narrow peak at ~3638 cm^{-1} is with a fixed FWHM in all spectra. The peak-fitting results were summarized in Table 2. It can be seen that the percentage of isolated surface hydroxyls in 6%-CoO/SiO_2 is 4.21% and reduces to 3.55% in Au/6%-CoO/SiO_2-2 and further to 1.06% in Au/6%-CoO/SiO_2-6. These IR results imply that the gold precursor prefers to interact with hydrogen-bonded

Table 2
The fraction of isolated surface hydroxyls in various catalysts.

Catalyst	Fraction of isolated surface hydroxyls (%)
SiO_2	1.25
6%-CoO/SiO_2	4.21
Au/6%-CoO/SiO_2-2	3.55
Au/6%-CoO/SiO_2-6	1.06
6%-CoO/SiO_2(500)	3.13
1%-Au/Au/6%-CoO/SiO_2(500)	2.36

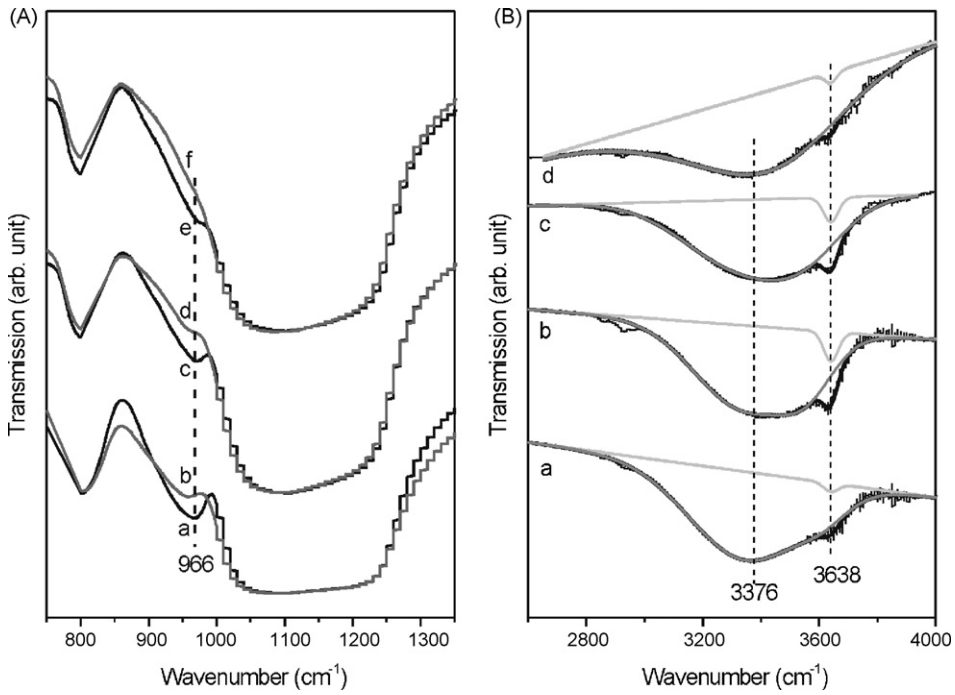

Fig. 8. (A) In situ infrared spectra of SiO_2 at RT (a), SiO_2 at 200 °C (b), 2%-$Co(OH)_2/SiO_2$ at RT (c), 2%-CoO/SiO_2 at 200 °C (d), 6%-$Co(OH)_2/SiO_2$ at RT (e), and 6%-CoO/SiO_2 at 200 °C (f); (B) in situ infrared spectra of SiO_2 (a), 6%-CoO/SiO_2 (b), Au/6%-CoO/SiO_2-2 (c), and Au/6%-CoO/SiO_2-6 (d) measured at 200 °C. The thin and solid lines in (B) correspond to the original and fitted infrared spectrum, respectively.

hydroxyls in $Co(OH)_2$ when the Au loading is low, therefore, most isolated hydroxyls in 6%-CoO/SiO_2 are preserved in the Au/6%-CoO/SiO_2-2 catalyst; with increasing Au loading, the gold precursor starts to interact with isolated hydroxyls in $Co(OH)_2$, which thus greatly reduces the percentage of isolated hydroxyls in the prepared Au/6%-CoO/SiO_2-6 catalyst. In combination with TEM results, it can be concluded that the gold precursor interacting with isolated hydroxyls in $Co(OH)_2$ eventually leads to the formation of fine Au nanoparticles.

Therefore, we propose a model (Scheme 1) to interpret the observed Au:CoO ratio-dependent size distribution of Au nanoparticles in Au/CoO/SiO_2 catalysts. Hydrogen-bonded hydroxyls in $Co(OH)_2$ can bind the gold precursor more strongly than isolated hydroxyls. During the DP process, the gold precursor preferentially deposits and interacts with hydrogen-bonded hydroxyls in $Co(OH)_2$ on SiO_2, forming clusters of gold species that nucleate and grow to large Au nanoparticles in the catalyst. Only after the occupation of hydrogen-bonded hydroxyls in $Co(OH)_2$ on SiO_2 can the gold precursor deposit and interact with isolated hydroxyls in $Co(OH)_2$, forming isolated gold species that reasonably forms fine Au nanoparticles in the catalyst. Qu et al. [51] previously observed that Ag^+ clusters interaction with hydrogen-bonded surface hydroxyls on SiO_2 formed large Ag nanoparticles whereas Ag^+ interaction with isolated hydroxyls on SiO_2 formed fine Ag nanoparticles. Therefore, our results clearly demonstrate that the distribution of surface hydroxyls on oxides might be an important factor to determine the size and catalytic activity of oxide-supported Au nanoparticles prepared by the DP method. Since the distribution of surface hydroxyls on oxides is difficult to be well controlled, it might be an important reason why the reproducible preparation of highly active Au/MO_x catalysts has sometimes been reported to be difficult by different research groups even the employed materials and preparation methods were similar [10].

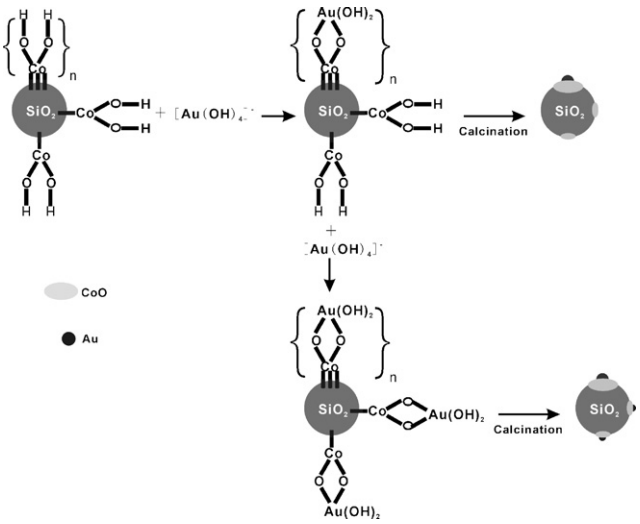

Scheme 1. A schematic illustration of the deposition of gold precursor on $Co(OH)_2/SiO_2$ and its influence on the structure of supported Au nanoparticles in Au/CoO/SiO_2 catalysts. $Co(OH)_2$ and $\{Co(OH)_2\}_n$ represent isolated $Co(OH)_2$ and $Co(OH)_2$ clusters with hydrogen-bonded hydroxyls on SiO_2, respectively.

Above model may provide a possibility of controlling the size of Au nanoparticles in Au/CoO/SiO_2 catalysts by controlling the relative amounts of hydrogen-bonded and isolated hydroxyls in $Co(OH)_2$ on SiO_2. $Co(OH)_2$ is transformed from $Co(NO_3)_2$ supported on SiO_2. Qu et al. [51] reported that the calcination of SiO_2 at 500 °C prior to the impregnation of $AgNO_3$ could selectively remove the hydrogen-bonded surface hydroxyls on the surface, which facilitates the exchange of Ag^+ with H^+ in isolated surface hydroxyls and thus improve the dispersion of prepared supported Ag nanoparticles. Therefore, a Au/CoO/SiO_2 catalyst(denoted as 1%-Au/6%-CoO/SiO_2(5 0 0)) was prepared in a similar way as the above Au/CoO/SiO_2 catalysts except that the SiO_2 support was calcined at 500 °C prior to the impregnation of $Co(NO_3)_2$. The Au and CoO loading in 1%-Au/6%-CoO/SiO_2(5 0 0) was analyzed by ICP-AES to be 0.9% and 5.4%, respectively. Interestingly, 1%-Au/6%-CoO/SiO_2(5 0 0) is active in low temperature

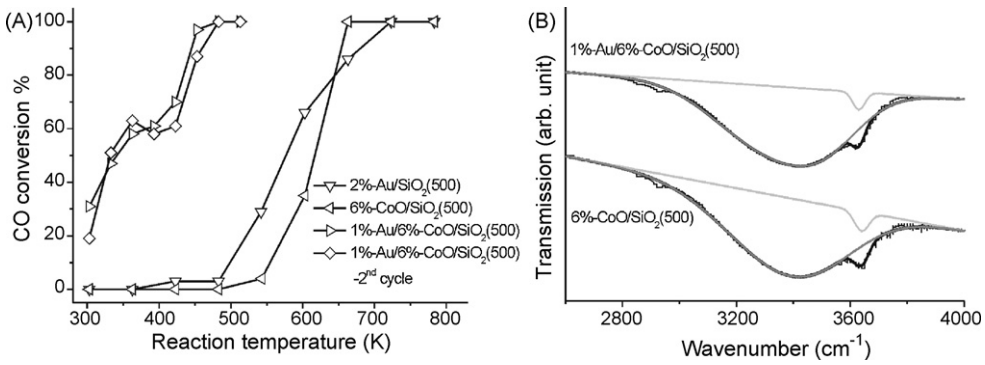

Fig. 9. (A) Catalytic performances of various catalysts supported on SiO_2 calcined at 500 °C; (B) in situ infrared spectra of 6%-CoO/SiO_2(5 0 0) and 1%-Au/6%-CoO/SiO_2(5 0 0) measured at 200 °C. The thin and solid lines in (B) correspond to the original and fitted infrared spectrum, respectively.

CO oxidation (Fig. 9A), demonstrating the presence of fine Au nanoparticles. Furthermore, its activity in the low reaction temperature range exhibits a volcano-shape dependence on the reaction temperature, and this dependence is reproducible for the tested 1%-Au/6%-CoO/SiO_2(5 0 0) catalyst. In contrast, Au/6%-CoO/SiO_2-1, Au/6%-CoO/SiO_2-2, and 1%-Au/CoO/SiO_2-4 catalysts with similar Au and CoO loadings are all not active in low temperature CO oxidation. These results demonstrate that the calcination of SiO_2 at 500 °C prior to the catalyst preparation could affect the structure of supported Au nanoparticles. We assume that the calcination of SiO_2 at 500 °C facilitates the formation of isolated Co^{2+} during the incipient wetness impregnation process and thus changes the hydroxyl distribution in $Co(OH)_2$ on SiO_2. As a result, even with a low Au loading, the gold precursor still has chances to deposit and interact with isolated hydroxyls on $Co(OH)_2$ during the DP process, leading to the formation of fine Au nanoparticles in 1%-Au/6%-CoO/SiO_2(5 0 0). Fig. 9B shows the O–H stretch vibration spectra of 6%-CoO/SiO_2(5 0 0) and 1%-Au/6%-CoO/SiO_2(5 0 0) measured at 200 °C. The peak-fitting results (Table 2) show that the percentage of isolated surface hydroxyls decreases from 3.13% in 6%-CoO/SiO_2(5 0 0) to 2.36% in 1%-Au/Au/6%-CoO/SiO_2(5 0 0), i.e. a 25% reduction. However, the percentage of isolated surface hydroxyls decreases from 4.21% in 6%-CoO/SiO_2 to 3.55% in Au/6%-CoO/SiO_2-2, i.e. only a 16% reduction. The data implies that more gold precursor should deposit and interact with isolated hydroxyls on $Co(OH)_2$ during the DP process of 1%-Au/6%-CoO/SiO_2(5 0 0) compared to the case of Au/6%-CoO/SiO_2-2. The 2%-Au/SiO_2(5 0 0) catalyst was also prepared but its activity in CO oxidation was similar to that of 2%-Au/SiO_2, which could be attributed to the disability of SiO_2 to stabilize fine Au nanoparticles.

Our results also demonstrate that the reaction pathway of CO oxidation catalyzed by Au/CoO/SiO_2 catalysts depends on the size of Au nanoparticles. Although with large Au nanoparticles, Au/6%-CoO/SiO_2-1, Au/6%-CoO/SiO_2-2, 1%-Au/CoO-SiO_2-3, 1%-Au/CoO-SiO_2-4, and 1%-Au/CoO-SiO_2-5 are much more active than Au/SiO_2, which could be attributed to the promotion effect of CoO. Schubert et al. [39] proposed that reducible transition metal oxide supports could activate and supply oxygen for CO oxidation catalyzed by supported Au nanoparticles and thus Au particles supported on reducible transition metal oxides were more active than those on inert oxides. However, 6%-CoO/SiO_2 itself only becomes active at 483 K, therefore, large Au nanoparticles and CoO should exert a synergetic effect on the activation of oxygen, that is, the dissociation of oxygen at high reaction temperatures. Therefore, we propose that the dissociation of oxygen occurs on the Au-CoO perimeter sites with lower activation energy in CO oxidation catalyzed by Au/CoO/SiO_2 catalysts with large Au nanoparticles. The CO oxidation then proceeds via the reaction of O(a) adsorbed on the Au-CoO perimeter sites with CO(a) adsorbed on the Au-CoO perimeter sites or on the Au surface.

Au/CoO/SiO_2 catalysts exhibit activity in low temperature CO oxidation when they contain fine Au nanoparticles. Haruta and Daté [2] observed different apparent activation energies for low temperature CO oxidation catalyzed by Au/TiO_2 at different reaction temperature regions and thus proposed a multireaction pathways including CO oxidation exclusively catalyzed by the Au surface, CO oxidation exclusively catalyzed by the Au atoms at the perimeter sites, and CO oxidation catalyzed by Au and TiO_2 at the perimeter sites. An interesting observation in our experiments is that the activity of 1%-Au/CoO/SiO_2-1, 1%-Au/CoO/SiO_2-2, and 1%-Au/6%-CoO/SiO_2(5 0 0) catalysts with fine Au nanoparticles in the low reaction temperature range exhibits a volcano-shape dependence on the reaction temperature whose origin could only be related to the detailed reaction pathway. We previously observed the similar volcano-shape activity-reaction temperature dependence for Au/ZnO/SiO_2 catalysts within the similar reaction temperature range [38], in which a weakly chemisorbed species was proposed to be involved in the reaction pathway and the temperature-dependent competition between the surface reaction and the desorption of this species was proposed to be responsible for the observed temperature-dependent activity. The current results further strengthen our previous argument.

4. Conclusions

By varying the Au:CoO ratio in Au/CoO/SiO_2 catalysts, we have successfully understood the DP process for the preparation of Au nanoparticles supported on CoO/SiO_2. The gold precursor preferentially deposits and interacts with hydrogen-bonded hydroxyls in $Co(OH)_2$ on SiO_2, forming clusters of gold species on the surface that eventually grow into large Au nanoparticles; after then, the gold precursor deposits and interacts with the isolated hydroxyls in $Co(OH)_2$, forming isolated Au species on the surface that leads to the formation of fine Au nanoparticles in the catalyst. Therefore Au/CoO/SiO_2 catalysts with low Au:CoO ratios only contain large Au nanoparticles and are active in catalyzing CO oxidation at high temperatures; with increasing Au:CoO ratio, Au/CoO/SiO_2 catalysts are with fine Au nanoparticles and become active in low temperature CO oxidation. The calcination of SiO_2 at 500 °C prior to the catalyst preparation can alter the structure of Au nanoparticles in Au/CoO/SiO_2 catalysts by changing the distribution of hydrogen-bonded and isolated hydroxyls in $Co(OH)_2$. Our results provide direct evidence that the distribution of surface hydroxyls on supports has great influence on the preparation of active supported Au catalysts, which is of great interest in the fundamental understanding of Au nanocatalysis.

Acknowledgments

The authors acknowledge financial support from National Natural Science Foundation of China (NSFC20773113), MOE program for PCSIRT (IRT0756) and MPG-CAS partner group.

Appendix A. Supplementary data

Supplementary data associated with this article can be found, in the online version, at doi:10.1016/j.molcata.2010.01.010.

References

[1] M. Haruta, N. Yamada, T. Kobayashi, S. Iijima, J. Catal. 115 (1989) 301.
[2] M. Haruta, M. Daté, Appl. Catal. A 222 (2001) 427.
[3] A.S.K. Hashmi, G.J. Hutchings, Angew. Chem. Int. Ed. 45 (2006) 7896.
[4] G.J. Hutchings, Catal. Today 122 (2007) 196.
[5] G.J. Hutchings, Gold Bull. 29 (1996) 123.
[6] G.C. Bond, D.T. Thompson, Gold Bull. 33 (2000) 41.
[7] M. Haruta, Stud. Surf. Sci. Catal. 145 (2003) 31.
[8] R. Meyer, C. Lemire, Sh.K. Shaikhutdinov, H.J. Freund, Gold Bull. 37 (2004) 72.
[9] M.S. Chen, D.W. Goodman, Catal. Today 111 (2006) 22.
[10] M.C. Kung, R.J. Davis, H.H. Kung, J. Phys. Chem. C 111 (2007) 11767.
[11] K. Qian, H.X. Sun, W.X. Huang, J. Fang, S.S. Lv, B. He, Z.Q. Jiang, S.Q. Wei, Chem. Eur. J. 14 (2008) 10595.
[12] M. Valden, X. Lai, D.W. Goodman, Science 281 (1998) 1647.
[13] H. Häkkinen, S. Abbet, A. Sanchez, U. Heiz, U. Landman, Angew. Chem. Int. Ed. 42 (2003) 1297.
[14] A. Del Vitto, G. Pacchioni, F. Delbecq, P. Sautet, J. Phys. Chem. B 109 (2005) 8040.
[15] M.S. Chen, D.W. Goodman, Acc. Chem. Res. 39 (2006) 739.
[16] Z.Q. Jiang, W.H. Zhang, L. Jin, X. Yang, F.Q. Xu, J.F. Zhu, W.X. Huang, J. Phys. Chem. C 111 (2007) 12434.
[17] K. Okazaki, S. Ichikawa, Y. Maeda, M. Haruta, M. Kohyama, Appl. Catal. A 191 (2005) 45.
[18] P. Concepcion, S. Carrettin, A. Corma, Appl. Catal. A 307 (2006) 42.
[19] J.G. Wang, B. Hammer, Phys. Rev. Lett. 97 (2006) 136107.
[20] J.C. Fierro-Gonzalez, J. Guzman, B.C. Gates, Top. Catal. 44 (2007) 103.
[21] M. Haruta, Catal. Today 36 (1997) 153.
[22] G.R. Bamwenda, S. Tsubota, T. Nakamura, M. Haruta, Catal. Lett. 44 (1997) 83.
[23] F. Moreau, G.C. Bond, A.O. Taylor, Chem. Commun. (2004) 1642.
[24] R. Zanella, L. Delannoy, C. Louis, Appl. Catal. A 291 (2005) 62.
[25] A. Wolf, F. Schüth, Appl. Catal. A 226 (2002) 1.
[26] G.J. Hutchings, M.S. Hall, A.F. Carley, P. Landon, B.E. Solsona, C.J. Kiely, A. Herzing, M. Makkee, J.A. Moulijn, A. Overweg, J.C. Fierro-Gonzalez, J. Guzman, B.C. Gates, J. Catal. 242 (2006) 71.
[27] A.A. Herzing, C.J. Kiely, A.F. Carley, P. Landon, G.J. Hutchings, Science 321 (2008) 1331.
[28] J.H. Yang, J.D. Henao, C. Costello, M.C. Kung, H.H. Kung, J.T. Miller, A.J. Kropf, J.G. Kim, J.R. Regalbuto, M.T. Bore, H.N. Pham, A.K. Datye, J.D. Laeger, K. Kharas, Appl. Catal. A 291 (2005) 73.
[29] F. Moreau, G.C. Bond, A.O. Tayler, J. Catal. 231 (2005) 105.
[30] A.M. Venezia, G. Pantaleo, A. Longo, G.D. Carlo, M.P. Casaletto, F.L. Liotta, G. Deganello, J. Phys. Chem. B 109 (2005) 2821.
[31] M.P. Casaletto, A. Longo, A.M. Venezia, A. Martorana, A. Prestianni, Appl. Catal. A 302 (2006) 309.
[32] F. Arena, P. Famulari, G. Trunfio, G. Bonura, F. Frusteri, L. Spadaro, Appl. Catal. B 66 (2006) 81.
[33] C.K. Chang, Y.J. Chen, C.T. Yeh, Appl. Catal. A 174 (1998) 13.
[34] S.H. Overbury, L. Ortiz-Soto, H.G. Zhu, B. Lee, M.D. Amiridis, S. Dai, Catal. Lett. 95 (2004) 99.
[35] H.G. Zhu, C.D. Liang, W.F. Yan, S.H. Overbury, S. Dai, J. Phys. Chem. B 110 (2006) 10842.
[36] K. Qian, S.S. Lv, X.Y. Xiao, H.X. Sun, J.Q. Lu, M.F. Luo, W.X. Huang, J. Mol. Catal. A 306 (2009) 40.
[37] K. Qian, W.X. Huang, Z.Q. Jiang, H.X. Sun, J. Catal. 248 (2007) 137.
[38] K. Qian, W.X. Huang, J. Fang, S.S. Lv, B. He, Z.Q. Jiang, S.Q. Wei, J. Catal. 255 (2008) 269.
[39] M.M. Schubert, S. Hackenberg, A.C. van Veen, M. Muhler, V. Plzak, R.J. Behm, J. Catal. 197 (2001) 113.
[40] M. Okumura, S. Nakamura, S. Tsubota, T. Nakamura, M. Azuma, M. Haruta, Catal. Lett. 51 (1998) 53.
[41] M.A.P. Dekkers, M.J. Lippits, B.E. Nieuwenhuys, Catal. Today 54 (1999) 381.
[42] K. Qian, Z.Q. Jiang, W.X. Huang, J. Mol. Catal. A 264 (2007) 26.
[43] R. Riva, H. Miessner, R. Vitali, G. Del Piero, Appl. Catal. A 196 (2000) 111.
[44] M. Voß, D. Borgmann, G. Wedler, J. Catal. 212 (2002) 10.
[45] A. Pantelouris, G. Küper, J. Hormes, C. Feldmann, M. Jansen, J. Am. Chem. Soc. 117 (1995) 11749.
[46] S.J. Lee, A. Gavriilidis, J. Catal. 206 (2002) 305.
[47] S. Wang, K. Qian, X.Z. Bi, W.X. Huang, J. Phys. Chem. C 113 (2009) 6505.
[48] B.F. Boccuzzi, S. Coluccia, G. Ghiotti, C. Morterra, A. Zecchina, J. Phys. Chem. 82 (1978) 1298.
[49] C.J. Jia, P. Massiani, D. Barthomeuf, J. Chem. Soc. Faraday Trans. 93 (1993) 3659.
[50] Y.C. Zhu, H.L. Li, Y. Koltypin, A. Gedanken, J. Mater. Chem. 12 (2002) 729.
[51] Z.P. Qu, W.X. Huang, S.T. Zhou, H. Zheng, X.M. Liu, M.J. Cheng, X.H. Bao, J. Catal. 234 (2005) 33.